

Curve fitting on a quantum annealer for an advanced navigation method

Philipp Isserstedt , ^{*} Daniel Jaroszewski, ^{1, 2, } Wolfgang Mergenthaler, ^{1, } Felix Paul, ^{3, 4, } and Bastian Harrach , ^{2, }

¹*FCE Frankfurt Consulting Engineers GmbH, Bessie-Coleman-Str. 7, 60549 Frankfurt am Main, Germany*

²*Institut für Mathematik, Goethe-Universität Frankfurt, Robert-Mayer-Str. 10, 60325 Frankfurt am Main, Germany*

³*AnaQor AG, Keithstr. 6, 10787 Berlin, Germany*

⁴*DLR-Institut für Weltraumforschung, Rutherfordstr. 2, 12489 Berlin, Germany*

We explore the applicability of quantum annealing to the approximation task of curve fitting. To this end, we consider a function that shall approximate a given set of data points and is written as a finite linear combination of standardized functions, e.g., orthogonal polynomials. Consequently, the decision variables subject to optimization are the coefficients of that expansion. Although this task can be accomplished classically, it can also be formulated as a quadratic unconstrained binary optimization problem, which is suited to be solved with quantum annealing. Given the size of the problem stays below a certain threshold, we find that quantum annealing yields comparable results to the classical solution. Regarding a real-world use case, we discuss the problem to find an optimized speed profile for a vessel using the framework of dynamic programming and outline how the aforementioned approximation task can be put into play.

Mathematics Subject Classification (2020): 65D10, 81P68, 90C39

I. INTRODUCTION

In 2020, the International Maritime Organization issued a recommendation to navigate just in time such that fuel consumption is minimized while arrival at the destination is guaranteed to be on time [1]. In this case, the approximation corresponds to an optimal speed profile for a vessel along a given trajectory in the sense that fuel consumption is minimized while arrival at the destination is guaranteed to be just in time. The given task is in fact an element of variational calculus and functional analysis. If one discretizes the problem in an attempt to generate a discrete sequence of speed values to support those objectives, one quickly ends up in the domain of dynamic programming and finds the Bellman equation to be a highly valuable tool [2–10].

Using dynamic programming to address large real-world use cases numerically necessitates a discretization of the problem’s state space. As a consequence, this entails an error in the accuracy of the so-called value function, which is the solution of the Bellman equation, and it is common practice to employ approximation techniques; see, e.g., Refs. [10, 11] and references therein.

One of the most fundamental approximation tasks is curve fitting, where a function is sought that approximates a given set of data, i.e., the difference between the observed data and the approximation shall become minimal. In this work, we formulate curve fitting as a quadratic unconstrained binary optimization (QUBO) problem [12, 13] that is suited to be solved with quantum computing—particularly quantum annealing [14–27].

Furthermore, in this context we discuss the task of finding an optimized speed profile for a vessel in the sense of minimal fuel consumption while arriving just in time using the framework of dynamic programming. Having the voyage of a vessel in mind, it might very well be the case that finding an optimized speed profile requires a lot of support points in order to densely discretize the state space, especially as soon as the latter becomes high-dimensional, and approximations are practically inevitable. Here, we use the QUBO formulation of curve fitting solved on a quantum annealer to approximate the value function with respect to its dependency on the state space variable.

With quantum computing currently being an emerging technology still in its infancy, we do not expect to outperform a conventional computer. Particularly in view of the fact that the only current commercially available quantum annealing devices manufactured by D-Wave [24, 28–37] are not full-fledged enough yet, and it is a priori not clear whether their use will result in practical advantages for a specific problem [26, 27, 38, 39]. Other application- and industry-focused development toward quantum annealing devices is carried out by, e.g., the NEC Corporation [40–42] and Qilimanjaro Quantum Tech [43, 44]. There are also quantum annealing-inspired devices tailored to solve QUBO problems, e.g., the coherent Ising machine [45, 46].

Nevertheless, in our opinion it is worth to explore to what extent quantum annealing can be applied to real-world use cases that arise in an application- and industry-focused environment (see Ref. [27] for an overview) and to judge the quality of the solutions compared to classical methods. This work lies within that scope.

The remainder of this article is organized as follows. In Section II, we formulate curve fitting as a QUBO and present our numerical results in Section III. After that, Section IV focuses on finding an optimized speed profile using dynamic programming, and we finally conclude in Section V.

^{*} philipp.isserstedt@frankfurtconsultingengineers.de

[†] daniel.jaroszewski@frankfurtconsultingengineers.de

[‡] wolfgang.mergenthaler@frankfurtconsultingengineers.de

[§] felix.paul@dlr.de

[¶] harrach@math.uni-frankfurt.de

II. CURVE FITTING AS A QUBO

Let $X, Y \subset \mathbb{R}$, $n \in \mathbb{N}$, and $\{(x_i, y_i)\}_{i=0}^{n-1} \subset X \times Y$ the observed data points. The task is to find an optimal fit function $f^*: X \rightarrow Y$ in the sense that the sum of squares of the differences between the observed data y_i and approximated values $f^*(x_i)$ is minimized (method of least squares) [47]. With \mathcal{F} denoting a suitable function space, e.g., $\mathcal{F} = \{f: \mathbb{R} \rightarrow \mathbb{R} \mid f \text{ continuous}\}$, we are concerned with the optimization problem

$$\min_{f \in \mathcal{F}} \sum_{i=0}^{n-1} (y_i - f(x_i))^2, \quad (1)$$

whose solution is the desired optimal fit f^* .¹ For example, if $f(x) = a_0 + a_1 x$, the minimization task (1) corresponds to identifying the optimal parameters $a_0^*, a_1^* \in \mathbb{R}$ for an ordinary simple linear regression model.

Here, we allow for a more general expression for f and express it as a finite linear combination of standardized functions $\{\phi_j: X \rightarrow Y\}_{j=0}^{m-1} \subset \mathcal{F}$, $m \in \mathbb{N}$, i.e.,

$$f(x) = \sum_{j=0}^{m-1} c_j \phi_j(x) \quad (2)$$

with $c_j \in \mathbb{R}$. Finding an optimal fit f^* thus translates into finding optimal coefficients c_j^* (for given ϕ_j). For example, such expansions are frequently employed within a certain area of high-energy physics where they aid to handle the numerical complexity of the occurring equations [48, 49]. Two customary choices for ϕ_j are:

(i) orthogonal polynomials such as Chebyshev polynomials. The first kind of the latter, T_j , are defined via the recurrence relation

$$T_j(x) = 2xT_{j-1}(x) - T_{j-2}(x) \quad (3)$$

for $j \in \mathbb{N}_{>1}$ with $T_1(x) = x$ and $T_0(x) = 1$ [50];

(ii) triangular functions Λ_j that yield a piecewise-linear approximation. They are defined with respect to supporting points $\tilde{x}_0 < \dots < \tilde{x}_{m-1}$, $m \geq 2$, with $\tilde{x}_0 = x_0$ and $\tilde{x}_{m-1} = x_{n-1}$ according to

$$\Lambda_j(x) = \begin{cases} \frac{x - \tilde{x}_{j-1}}{\tilde{x}_j - \tilde{x}_{j-1}} & \text{if } x \in [\tilde{x}_{j-1}, \tilde{x}_j) \\ \frac{\tilde{x}_{j+1} - x}{\tilde{x}_{j+1} - \tilde{x}_j} & \text{if } x \in [\tilde{x}_j, \tilde{x}_{j+1}) \\ 0 & \text{otherwise} \end{cases} \quad (4)$$

¹ By construction of minimizing residuals, the least squares method always yields a solution, i.e., an optimal fit f^* always exists. In our case, where the fit function is written as a finite linear combination of standardized functions according to Eq. (2), the solution is unique if the matrix W , defined later in Eq. (6), has full rank.

for $j = 0, \dots, m-1$, where it is understood that only the first (second) branch defines the nonzero values of the last (first) triangular function $\Lambda_{j=m-1}$ ($\Lambda_{j=0}$).

A. Classical solution

We aim to determine the expansion coefficients c_j in Eq. (2) according to the least-squares principle as given by the optimization problem (1). With the abbreviations (where $j, k = 0, \dots, m-1$)

$$b_j = \sum_{i=0}^{n-1} y_i \phi_j(x_i), \quad (5)$$

$$W_{jk} = \sum_{i=0}^{n-1} \phi_j(x_i) \phi_k(x_i), \quad (6)$$

vectors $c = [c_0, \dots, c_{m-1}]^\top \in \mathbb{R}^m$, $b = [b_0, \dots, b_{m-1}]^\top \in \mathbb{R}^m$, and the symmetric matrix $W \in \mathbb{R}^{m \times m}$ with entries W_{jk} , the optimization problem upon inserting Eq. (2) into (1) now takes the form

$$\begin{cases} \min_{c \in \mathbb{R}^m} Z(c), \\ Z(c) = c^\top W c - 2c^\top b. \end{cases} \quad (7)$$

The optimal weight coefficient vector c^* thus follows from

$$\nabla Z(c^*) = 2(Wc^* - b) \stackrel{!}{=} 0 \quad (8)$$

and is explicitly given by

$$c^* = W^{-1}b \quad (9)$$

provided W is invertible. If this is not the case, in practice one could resort to its Moore–Penrose pseudoinverse [51].

B. Quantum annealing-oriented approach

Starting from the objective function as given in (7) in its expanded form

$$Z(c) = \sum_{j=0}^{m-1} \sum_{k=0}^{m-1} c_j W_{jk} c_k - 2 \sum_{j=0}^{m-1} c_j b_j, \quad (10)$$

we have a quadratic function in the components of c . In order to express the optimization problem (7) as a QUBO, whose decision variables' domain is the set $\{0, 1\}$, we write each coefficient c_j in binary fixed-point format and use two's complement to represent negative values. This yields the following expression for the coefficients:

$$c_j = \sum_{r=0}^{d-1} \psi_{jr} \sigma_r 2^{r-p}, \quad (11)$$

where $\psi_{jr} \in \{0, 1\}$, $d \in \mathbb{N}$ defines how many binary digits are used, $p = 0, \dots, d-1$ indicates the location of the fixed decimal point, and

$$\sigma_r = \begin{cases} -1 & \text{if } r = d-1 \\ 1 & \text{otherwise} \end{cases} \quad (12)$$

accounts for two's complement, i.e., the most significant bit enters the sum with a negative sign. For example, for $p=0$, Eq. (11) allows to represent all integers between $-(2^{d-1})$ and $2^{d-1} - 1$. The quantities ψ_{jr} are then the new decision variables represented by the qubit states of a quantum annealing device.

In principle, one could choose different values for d and p for each coefficient c_j matching the individual order of magnitude and location of the decimal point of each coefficient. In practice, however, these are (usually) not known a priori. Thus, and for the sake of simplicity, we choose the same d and p for all coefficients.

Now, inserting Eq. (11) into (10) yields a new objective function depending on $\psi = [\psi_{00}, \psi_{01}, \dots]^\top \in \{0, 1\}^{md}$, i.e., on all coefficients of the binary representation of the expansion coefficients; to wit

$$Z(\psi) = \sum_{j,k=0}^{m-1} \sum_{r,s=0}^{d-1} \psi_{jr} \psi_{ks} \sigma_r \sigma_s W_{jk} 2^{r+s-2p} - \sum_{j=0}^{m-1} \sum_{r=0}^{d-1} \psi_{jr} \sigma_r b_j 2^{r-p+1}. \quad (13)$$

This equation can also be written as

$$Z(\psi) = \sum_{\mu, \nu=0}^{md-1} \psi_\mu W'_{\mu\nu} \psi_\nu - \sum_{\mu=0}^{md-1} \psi_\mu b'_\mu, \quad (14)$$

where $\psi_\mu = \psi_{\mu\bar{\mu}}$, $b'_\mu = 2^{\bar{\mu}-p+1} \sigma_{\bar{\mu}} b_{\bar{\mu}}$, and $W'_{\mu\nu} = 2^{\bar{\mu}+\bar{\nu}-2p} \sigma_{\bar{\mu}} \sigma_{\bar{\nu}} W_{\bar{\mu}\bar{\nu}}$ with $\bar{\mu} = \lfloor \mu/d \rfloor$ and $\bar{\mu} = \mu \bmod d$ (analogously for ν). b'_μ and $W'_{\mu\nu}$ are the entries of the quantities $b' \in \mathbb{R}^{md}$ and $W' \in \mathbb{R}^{(md) \times (md)}$, respectively. These definitions allow us to write the objective function in a rather compact form:

$$Z(\psi) = \psi^\top W' \psi - \psi^\top b'. \quad (15)$$

Finally, in order to cast this objective function into the canonical QUBO form, we exploit that the entries of the binary vector ψ are idempotent, $\psi_\mu^2 = \psi_\mu$ for all $\mu = 0, \dots, md-1$. The linear term $\psi^\top b'$ can therefore be written as a contribution that is subtracted from the diagonal elements of W' . Thus, our final expression for the least-squares optimization problem (1) written as a QUBO reads

$$\min_{\psi \in \{0,1\}^{md}} \psi^\top Q \psi \quad (16)$$

with the QUBO matrix

$$Q = W' - \text{diag}(b'_0, \dots, b'_{md-1}) \in \mathbb{R}^{(md) \times (md)}. \quad (17)$$

In a last step, the solution ψ^* of the QUBO problem is plugged into Eq. (11) to obtain the actual, real-valued optimal coefficients $c_j^* = \sum_r \psi_{jr}^* \sigma_r 2^{r-p}$.

Apparently, the number of required qubits, i.e., the size of the QUBO problem, depends only on the number of standardized functions m used for the expansion of the fit function, see Eq. (2), and the number of digits d used for the binary representation of the expansion coefficients. In other words, the size of the QUBO matrix Q is independent of the number of the to-be-approximated data points n (see Eq. (1)); the latter enters only implicitly in the course of the determination of the entries of Q (see Eqs. (5) and (6)).

III. NUMERICAL EXPERIMENTS

In the following, we present and discuss our numerical results of the curve fitting task by means of a QUBO problem as described above.

Since we shall compare results obtained on a classical computer using a tabu search [52, 53] with results from a D-Wave quantum annealing device, we sketch very briefly the idea behind the latter (see, e.g., Refs. [24, 36, 37, 54] and references therein for more details). Based on the concept of adiabatic quantum computing [25] and relaxing some of its properties/conditions to facilitate a feasible realization, quantum annealing is a metaheuristic method [24] to find low-energy solutions—including the ground state(s)—of an Ising spin model [55, 56]. For a system of spins $s = [s_0, \dots, s_{N-1}]^\top \in \{-1, 1\}^N$, $N \in \mathbb{N}$, a ground state is a spin configuration that globally minimizes the objective function

$$Z_{\text{Ising}}(s) = \sum_{i=0}^{N-1} \sum_{j=i+1}^{N-1} J_{ij} s_i s_j + \sum_{i=0}^{N-1} h_i s_i, \quad (18)$$

where $J_{ij} \in \mathbb{R}$ and $h_i \in \mathbb{R}$ denote the nearest-neighbor interaction between the i^{th} and j^{th} spin (coupling strength) and an external magnetic field acting on the i^{th} spin (qubit bias), respectively.

The connection to the corresponding QUBO model with objective function $Z_{\text{QUBO}}(z) = z^\top R z$ with $z \in \{0, 1\}^N$ and an upper-triangular matrix $R \in \mathbb{R}^{N \times N}$ is established by the transformation $s_i = 2z_i - 1$ for $i = 0, \dots, N-1$. The off- and on-diagonal entries of R are appropriately mapped onto the coupling strengths and qubit biases, respectively. It is then straightforward to show that the Ising and QUBO objective functions differ only by an additive constant in the sense that

$$Z_{\text{Ising}}(s)|_{s_i=2z_i-1} = Z_{\text{QUBO}}(z) + \text{const.}, \quad (19)$$

i.e., an approximate or exact solution of a given QUBO problem can be equivalently obtained by finding low-energy or ground states of an Ising model, respectively.

A. Sample data

Before we continue with our actual results, we define the sample data $\{(x_i, y_i)\}_{i=0}^{n-1}$ (see Section II) that shall be used for our numerical experiments. The abscissa values are evenly spaced over the unit interval according to

$$x_i = \frac{i}{n-1} \in [0, 1]. \quad (20)$$

For the ordinates, we choose the following four different types:

$$\text{linear: } y_i = \frac{1}{2}x_i + 1 + \varepsilon_i, \quad (21)$$

$$\text{quadratic: } y_i = \frac{3}{4}x_i^2 + \varepsilon_i, \quad (22)$$

$$\text{cubic: } y_i = \frac{3}{4}x_i^3 + \frac{1}{4}x_i + \varepsilon_i, \quad (23)$$

$$\text{trigonometric: } y_i = \sin(2\pi x_i) \cos(2\pi x_i) + \varepsilon_i, \quad (24)$$

which are all distorted by noise ε_i . At each ordinate y_i , the latter is a random variable drawn from a normal distribution centered about zero with variance $(0.03)^2$, i.e., $\varepsilon_i \sim \mathcal{N}(\mu = 0, \sigma^2 = (0.03)^2)$ for $i = 0, \dots, n-1$.

In order to compare results, we use either the absolute percentage error (APE)

$$\text{ape}(a, b) = \frac{|a - b|}{\max\{|a|, \delta\}} \times 100 \quad (25)$$

with $a, b \in \mathbb{R}$, $\delta > 0$ or the root mean squared error (RMSE)

$$\text{rmse}(f^*) = \sqrt{\frac{1}{n} \sum_{i=0}^{n-1} (y_i - f^*(x_i))^2}, \quad (26)$$

where $f^*(x) = \sum_{j=0}^{m-1} c_j^* \phi_j(x)$ is a given optimal fit with optimal expansion coefficients c_j^* obtained from solving the least-squares optimization problem (see Eqs. (1) and (2)). Equation (26) aggregates the squared differences between the actual and approximated values for each sample data point—the very same measure that is minimized by the method of least squares—and is thus well-suited to compare optimal least-squares fits f^* obtained via different techniques (see Sections II A and II B).

Furthermore, we always normalize the ordinate values to the unit interval before the optimal fit is computed. That is, the least-squares method actually operates on min-max-normalized data points $\{(x_i, y'_i)\}_{i=0}^{n-1}$ with

$$y'_i = \frac{y_i - y_{\min}}{y_{\max} - y_{\min}} \in [0, 1], \quad (27)$$

where $y_{\min} = \min_i y_i$ and $y_{\max} = \max_i y_i$. Thus, all optimal expansion coefficients c_j^* presented here are understood to be obtained with respect to min-max-normalized data y'_i .

Now, in the following we consider three different standardized functions ϕ_j for the expansion (2) of the fit function, apply them to our sample data, and discuss the quality of the solutions obtained via different strategies as well as the influence of certain parameters.

B. Triangular functions

We begin with triangular functions as defined in Eq. (4), $\phi_j = \Lambda_j$, i.e., the fit function is given by

$$f(x) = c_0 \Lambda_0(x) + \dots + c_{m-1} \Lambda_{m-1}(x), \quad (28)$$

and the least squares optimization problem thus explicitly reads

$$\min_{c \in \mathbb{R}^m} \sum_{i=0}^{n-1} \left(y_i - \sum_{j=0}^{m-1} c_j \Lambda_j(x_i) \right)^2. \quad (29)$$

First, we consider the simple yet important case of linear regression. To this end, we choose $n = 64$ and the linear sample data (21). Furthermore, we set $m = 2$, which implies that the two supporting points of the triangular functions (see Eq. (4)) are simply the first and last abscissa values (20) of the sample data, respectively, i.e., $\tilde{x}_0 = x_0 = 0$ and $\tilde{x}_1 = x_{n-1} = 1$. This results in a fit function $f(x) = c_0 \Lambda_0(x) + c_1 \Lambda_1(x)$ that is a straight line across the whole abscissa interval $[0, 1]$ of our sample data. For the corresponding QUBO formulation of the problem, we choose $d = 10$ and $p = d - 2 = 8$, which results in a QUBO matrix of size $md \times md = 20 \times 20$.

In Tab. I, we show our results for the optimal linear regression parameters c_0^* and c_1^* obtained classically by (naive) matrix inversion according to Eq. (9) and by solving the corresponding QUBO as given in Eq. (16); we also show the APE (see Eq. (25)) of the optimal coefficients obtain via a QUBO with respect to the classical results. The QUBO is solved by means of a tabu search as well as by quantum annealing on a D-Wave quantum processing unit.² Comparing the three solutions, we find that all agree up to the second decimal point. The QUBO solution found by the tabu search is particularly close to the exact classical solution, agreeing up to the third decimal point. Though the quantum annealing solution differs more noticeably, it is still in good agreement with the two other results. Furthermore, we find qualitatively similar results if we replace the numerical coefficients in the linear sample data (21) by other values, e.g., randomly drawn

² For the tabu search, we used the *MST2* multi-start tabu algorithm of Ref. [57]. Regarding quantum annealing for solving the QUBO, we used D-Wave's *Advantage2* system. In particular, we performed 100 runs with 100 reads each with an annealing time of 200 microseconds to collect potential solution candidates, yielding 10000 samples in total, and finally took the lowest-energy solution. This setup is used throughout the whole section whenever a QUBO problem is solved via tabu search or quantum annealing.

Table I. Optimal linear regression parameters obtained classically and by solving a QUBO. Also shown are the absolute percentage errors (APE) of the optimal parameters obtained from the QUBO with respect to the classical ones.

	c_0^*	c_1^*	APE c_0^* [%]	APE c_1^* [%]
Classical (matrix inversion)	0.010664	0.978332	—	—
QUBO (tabu search)	0.010742	0.978516	0.73	0.02
QUBO (quantum annealing)	0.011719	0.977539	9.89	0.08

Table II. Same as Tab. I but with the linear sample data now given by $y_i = -x_i/4 + 1/3 + \varepsilon_i$.

	c_0^*	c_1^*	APE c_0^* [%]	APE c_1^* [%]
Classical (matrix inversion)	0.874487	0.200203	—	—
QUBO (tabu search)	0.875000	0.200195	0.06	0.004
QUBO (quantum annealing)	0.872070	0.196289	0.28	1.96

Table III. APE between the RMSE of the optimal classical solution f_{cl}^* and the optimal QUBO solutions f_{tb}^* and f_{qa}^* obtained via tabu search and quantum annealing, respectively, for different values of n . The underlying sample data set is the linear one (Eq. (21)) and a linear regression is used for the approximation.

n	ape(rmse(f_{cl}^*), rmse(f_{tb}^*)) [%]	ape(rmse(f_{cl}^*), rmse(f_{qa}^*)) [%]
64	2.88×10^{-4}	2.23×10^{-2}
128	3.64×10^{-4}	4.50×10^{-2}
256	1.10×10^{-4}	1.22×10^{-2}
512	1.09×10^{-4}	1.71×10^{-2}
1024	6.80×10^{-4}	3.16×10^{-2}

from $[-1, 1]$. As an example, Tab. II shows the results for a different set of linear sample data.

Thus, in the case of linear regression, our results indicate that formulating curve fitting as a QUBO problem indeed works and yields a solution in satisfying agreement with the classical one. They also suggest that quantum annealing in its current state is in principle able (within limits) to deliver promising and practically usable results for this continuous problem.³

It is furthermore instructive to investigate the influence of certain parameters on the solutions. In Tab. III, we show the APE between the RMSE of the optimal classical solution f_{cl}^* and the optimal QUBO solutions f_{tb}^* and f_{qa}^* obtained via tabu search and quantum annealing, respectively, for different values of the number of sample data points n (again for the case of linear regression with sample data (21)). We conclude that the number of to-

be-approximated data points has a negligible influence on the solution quality. This is expected because n enters only implicitly in the course of determining the entries of the QUBO matrix (see Eqs. (5) and (6)) while its size is given by $md \times md$, see Eq. (17), i.e., only determined by m and d . We find the same result if we use our other sample data sets instead of the linear one. Therefore, we fix $n = 64$ for the remainder of this section.

In Fig. 1, we show the RMSE of the tabu (red squares) and quantum annealing (green diamonds) solutions f_{tb}^* and f_{qa}^* , respectively, as a function of d , the number of digits that is used for the binary fixed-point format of the coefficients c_j , see Eq. (11), with $p = d - 1$ fixed. Furthermore, we show the RMSE of the classical solution f_{cl}^* , which is exact in the sense of numerical precision and thus independent of d . Here, we use the cubic sample data (23) and $m = 4$, i.e., we are beyond linear regression and have a truly piecewise-linear fit of the form $f(x) = c_0\Lambda_0(x) + \dots + c_3\Lambda_3(x)$ that is not just a straight regression line. For $d \geq 8$, the tabu solutions are very close to the classical one and a further increase of d has only a negligible impact. The same holds for the quantum annealing solutions, though they are always less accurate than the corresponding tabu results. Both are only identical provided the QUBO matrix is small enough, namely for $d \leq 5$, which corresponds to a QUBO matrix of size

³ Because of the probabilistic (or stochastic) nature of quantum annealing and the fact that the quantum annealing device is a real (i.e., non-ideal) system—thus susceptible to thermal fluctuations and interactions with its environment—subsequent calculations with the same input may yield slightly different results. Based on our experiences and observations in the course of this work, the quantum annealing results presented here seem to be accompanied with an overall error of about five to ten percent.

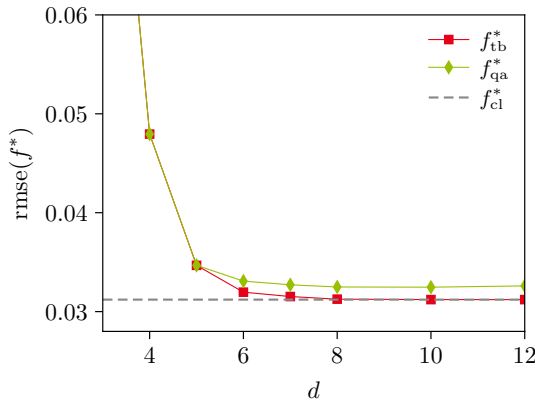


Figure 1. RMSE of the d tabu search (red squares, f_{tb}^*) and quantum annealing (green diamonds, f_{qa}^*) solutions as a function of d . The RMSE of the exact, d -independent classical solution f_{cl}^* is shown as a gray dashed line. Lines between data points are shown to guide the eye. The underlying sample data set is the cubic one (Eq. (23)), and triangular functions with $m = 4$ are used for the approximation.

20 \times 20 or smaller. In our opinion, however, the quantum annealing solutions for larger QUBO sizes are still in acceptable agreement with the tabu and classical ones. We find qualitatively similar results if we use the quadratic sample data or if the numerical coefficients of the cubic data are randomly drawn from $[-1, 1]$. Therefore, $d = 8$ (with $p = d - 1$) seems to be sufficient for the binary fixed-point representation of the expansion coefficients c_j regarding the cases considered in this work. Furthermore, $d \in \{6, 7\}$ are reasonable compromises between accuracy and keeping the QUBO matrix as small as possible.

Last, we consider the case of varying m , i.e., how the solution quality depends on the number of triangular functions used for the curve fitting. This is an particularly interesting case because one usually chooses a sufficient numerical accuracy and simply increases m to the point where the data is sufficiently good approximated. Curve fitting with triangular functions is well-suited for that because the result is a piecewise-linear approximation (a polygonal chain), which is often used to approximate more complex curves or if the functional form of the to-be-approximated data is not immediately obvious. In Fig. 2, we show the RMSE of the tabu (red squares), quantum annealing (green diamonds), and classical (gray circles) solutions as a function of m , where the sample data sets are the trigonometric (left diagram) and quadratic ones (right diagram); again, $n = 64$, $d = 8$, and $p = d - 1 = 7$. First, we consider the left diagram. It shows the overall trend that the RMSE of the classical solution becomes smaller as m increases. Initially, the tabu and quantum annealing solutions follow that trend. For $m \geq 10$ (which corresponds to a QUBO matrix of size 80×80), however, the quantum annealing solution becomes worse with increasing m . The right diagram, though with a rather different underlying set of sample data (quadratic instead of trigonometric), shows the same qualitative behavior.

Quantitatively, noticeable differences and a continuous worsening of the quantum annealing solutions with increasing m already starts at $m = 8$, which corresponds to a QUBO matrix size of 64×64 .

We also tested other polynomial sample data as well as varied the numerical coefficients of the sample data used for Fig. 2 and found qualitatively similar results. This indicates that a QUBO size of about 60×60 to 80×80 seems to be the range above which D-Wave's current quantum annealing hardware fails to find a satisfying solution of the QUBO formulation of least squares curve fitting with triangular functions.

C. Chebyshev polynomials

Besides the triangular functions, we shall also consider Chebyshev polynomials of the first kind as defined in Eq. (3), $\phi_j = T_j$, i.e., the fit function is now given by

$$f(x) = c_0 + \sum_{j=1}^{m-1} c_j T_j(x) \quad (30)$$

and is a polynomial of degree m .

In Tab. IV, we show our results for fitting a quadratic Chebyshev polynomial (i.e., $m = 3$) to the quadratic sample data (22); again, $n = 64$, $d = 8$, and $p = d - 1 = 7$, which results in a QUBO matrix of size 24×24 . While the tabu solution is in acceptable agreement with the classical one, the quantum annealing solution deviates significantly. We find the same result for the cubic data (also with varying numerical coefficients) with a cubic Chebyshev polynomial ($m = 4$) as the fit function. In Fig. 3, we show the RMSE of the tabu (red squares) and quantum annealing (green diamonds) solutions f_{tb}^* and f_{qa}^* , respectively, as a function of d , the number of digits that is used for the binary fixed-point format of the expansion coefficients. Furthermore, we show the RMSE of the classical solution, which is independent of d , as a gray dashed line. The underlying sample data is the cubic one and the Chebyshev fit is of degree three, i.e., $m = 4$. We plot against d because we would like to keep the degree of the Chebyshev polynomial fixed while letting the QUBO matrix increase in size. While the tabu solution shows the expected behavior (cf. Fig. 1), we are not able to obtain a satisfying quantum annealing solution for problem sizes larger than 20×20 . This is in stark contrast to our findings for piecewise-linear curve fitting using triangular functions.

This seems to hint toward the limitations of D-Wave's current quantum annealing hardware for curve fitting with polynomials formulated as a QUBO. More precisely, the corresponding QUBO problem, which can be seen as a graph with logical qubits representing nodes that are connected by edges with weights given by the matrix elements of the QUBO matrix, needs to be mapped onto the so-called working graph of the quantum annealing device. Therefore, one might need several physical qubits

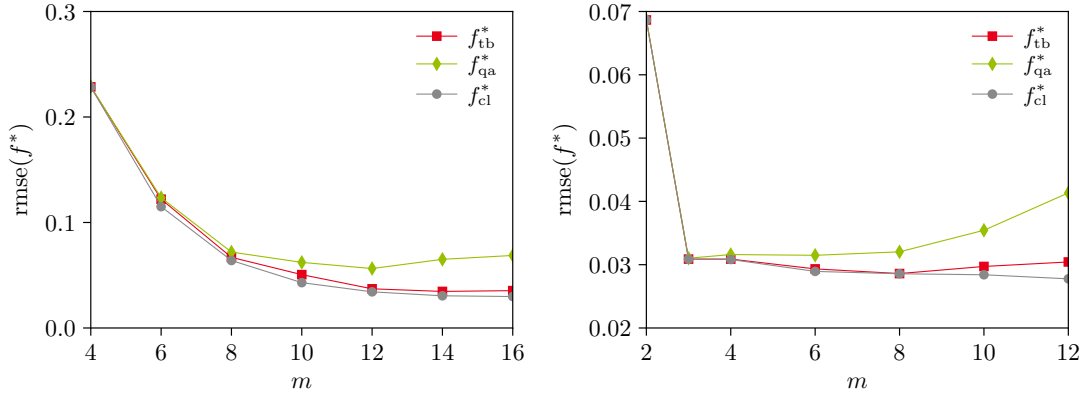


Figure 2. RMSE of the tabu search (red squares, f_{tb}^*), quantum annealing (green diamonds, f_{qa}^*) and classical (gray circles, f_{cl}^*) solutions as a function of m . The underlying sample data are the trigonometric (left diagram) and quadratic (right diagram) ones, respectively.

Table IV. Optimal expansion coefficients of the individual Chebyshev polynomials of a quadratic fit, obtained classically via matrix inversion and by solving a QUBO via tabu search as well as quantum annealing. Also shown are the APE of the optimal coefficients obtained from the QUBO with respect to the classical ones.

	c_0^*	c_1^*	c_2^*	APE c_0^* [%]	APE c_1^* [%]	APE c_2^* [%]
Classical (matrix inversion)	0.544598	-0.031799	0.499257	—	—	—
QUBO (tabu search)	0.523438	-0.039063	0.484375	3.89	22.84	2.98
QUBO (quantum annealing)	0.445313	-0.101563	0.421875	18.23	219.39	15.50

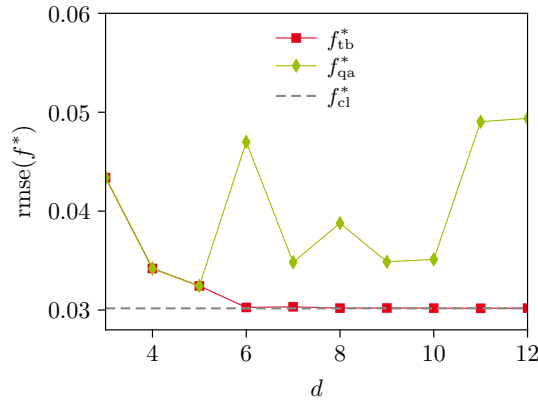


Figure 3. RMSE of the tabu search (red squares, f_{tb}^*) and quantum annealing (green diamonds, f_{qa}^*) solutions as a function of d . The RMSE of the exact, d -independent classical solution f_{cl}^* is shown as a gray dashed line. Lines between data points are shown to guide the eye. The underlying sample data set is the cubic one (Eq. (23)), and Chebyshev polynomials with $m = 4$ are used for the approximation.

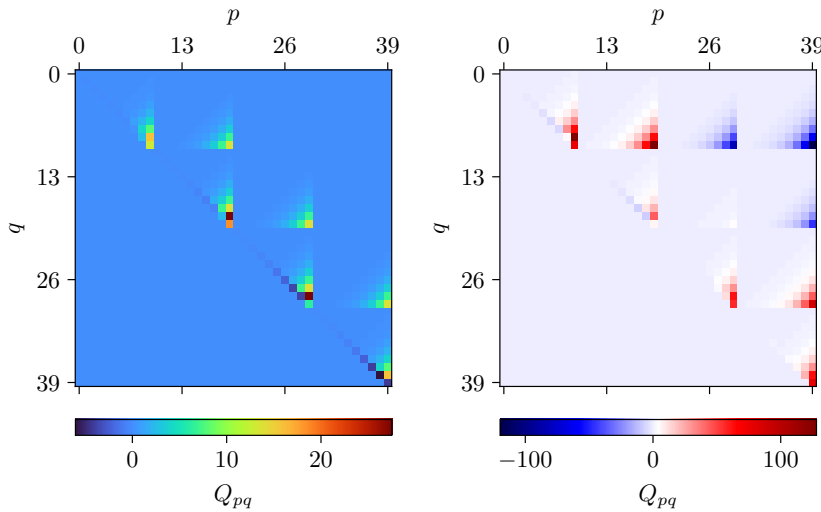


Figure 4. Heat map plots of exemplary QUBO matrices Q of piecewise-linear approximation with triangular functions (left) and Chebyshev polynomial approximation (right). Here, we display the upper-triangularized versions of these matrices since every QUBO problem can be written in a way such that Q is an upper-triangular matrix.

to represent one logical qubit. Particularly for highly-connected (dense) QUBO problems, this could yield an Ising model that exhibits a complicated low-energy landscape where the ground state is difficult to access. This would explain why we were not successful in obtaining a feasible Chebyshev approximation as soon as its QUBO matrix is larger than the above mentioned size of about 20×20 . Such a matrix is, as apparent from the right diagram of Fig. 4, indeed relatively highly connected.

The amount of nonvanishing off-diagonal elements of the QUBO matrix for least-squares curve fitting is solely determined by the standardized functions ϕ_j (keeping the underlying to-be-approximated data fixed); see Eq. (6). More precisely, in case of the Chebyshev approximation we deal with polynomials T_j whose support are the whole real line,

$$\text{supp}(T_j) = \mathbb{R} \quad (31)$$

for all j . Therefore, the resulting QUBO problem corresponds to a rather highly connected graph, and the matrix has many nonzero elements even far off the diagonal; see the right diagram of Fig. 4 for a graphical depiction. On the other hand, the QUBO matrix for a piecewise-linear approximation is always a band matrix, see the left diagram of Fig. 4, because the triangular functions Λ_j have compact support,

$$\text{supp}(\Lambda_j) = \begin{cases} [\tilde{x}_0, \tilde{x}_1] & \text{if } j = 0, \\ [\tilde{x}_{m-2}, \tilde{x}_{m-1}] & \text{if } j = m-1, \\ [\tilde{x}_{j-1}, \tilde{x}_{j+1}] & \text{otherwise.} \end{cases} \quad (32)$$

In our opinion, this explains why

- (i) we are unsuccessful in finding a satisfying quantum annealing solution for the Chebyshev approximation for QUBO matrices larger than a certain size;

- (ii) the Chebyshev solution is less accurate compared to the piecewise-linear approximation for feasible cases of the size of the QUBO problem.

Furthermore, another obstacle might be the order of magnitude of the elements of the QUBO matrix. These have to be mapped onto the coupling strengths and qubit biases of the Ising model, which are constrained by the physical limits of the quantum annealing hardware, i.e., the available ranges of couplings and biases as well as their coarseness. As a consequence, it might be the case that a complicated low-energy landscape cannot be “scanned” accurate enough by the current quantum annealing devices. Unfortunately, the actual values of these matrix elements are determined by the to-be-approximated data and the employed standardized functions ϕ_j and thus cannot be freely adjusted or altered.

We would like to emphasize that by solving the QUBO problems for piecewise-linear and Chebyshev approximations using a heuristic technique, e.g., tabu search or simulated annealing, we (almost) always find a solution in satisfying agreement with the classical one—even for sizes of the QUBO matrix for which the quantum annealing solution turned out to be unpractical. Thus, we are confident that a next-generation quantum annealing device will be capable of solving such QUBO problems.

Finally, we would like to mention that we always subjected the “raw” QUBO matrix to the quantum annealing process. It is well-known that dense QUBO problems are hard to solve, and a proper preprocessing of the QUBO matrix might improve the solution quality. Possible preprocessing steps are sparsification of the QUBO matrix or properly modifying/combining matrix elements [58–60], possibly resulting in a reduction in size and/or density of the problem. Another approach would be quantum annealing-inspired algorithms like SimCIM [61] or the

NGQ solver [62], which seem to be more robust against dense QUBO problems [62–64]. However, these investigations are beyond the scope of this work and deferred to possible future work.

IV. SPEED PROFILE OPTIMIZATION WITH DYNAMIC PROGRAMMING

In this section, we touch upon a real-world use case, with which we are currently concerned, where curve fitting can come in handy. Namely, a cargo vessel's voyage under the constraint of minimal fuel consumption while arriving at the destination at the requested time of arrival. Phrased differently, the aim is to find an optimized speed profile that minimizes fuel costs while arriving just in time. From our point of view, this task lends itself to be solved within the framework of dynamic programming [2–4]; see, e.g., Refs. [5–10] for comprehensive overviews. Work in that direction has been done regarding the optimal control of sailboats [65–67]. To our knowledge, however, dynamic programming is not used for maritime just-in-time navigation of cargo vessels yet, and we would like to leverage its use.

A. General formalism

More formally speaking, we consider a deterministic Markov decision process that starts at time $t = 0$ and terminates at $t = T$, where the time evolution is discrete in terms of integer time steps: $t = 0, \dots, T$. The process is characterized by sets $X_t \subset \mathbb{R}^k$ and $U_t \subset \mathbb{R}^l$, where $k, l \in \mathbb{N}$, that contain all states the process can be in and all actions that can be performed in order to change the current state, respectively, at time step t .⁴

The dynamics of the decision process, i.e., how the next state $x_{t+1} \in X_{t+1}$ is obtained from the previous one $x_t \in X_t$ by performing a certain action $u_t \in U_t$, are governed by a transition function $\Gamma_t: X_t \times U_t \rightarrow X_{t+1}$; that is,

$$x_{t+1} = \Gamma_t(x_t, u_t). \quad (33)$$

The immediate costs that occur if the action u_t is performed while being in state x_t are given by a cost function $C_t: X_t \times U_t \rightarrow \mathbb{R}$. This motivates the definition of a value function $V_t: X_t \times U_t \times \dots \times U_{T-1} \rightarrow \mathbb{R}$, which is given by

$$V_t(x_t, u_t, \dots, u_{T-1}) = \sum_{s=t}^{T-1} C_s(x_s, u_s) + D(x_T), \quad (34)$$

⁴ In general, the actions depend on the state $x_t \in X_t$ of the process, i.e., $U_t = U_t(x_t)$. However, in terms of notation, we omit this dependency for the sake of brevity.

where $D: X_T \rightarrow \mathbb{R}$ encodes terminal costs that occur at the end of the process. The value function is a measure for how cost-effectively the decision process has been if started at time step t with initial state x_t and running until the end by virtue of a given sequence of actions u_t, \dots, u_{T-1} . The states x_{t+1}, \dots, x_T in Eq. (34) are generated according to the temporal evolution defined by the process' dynamics (33).

The goal is to find optimal actions u_t^*, \dots, u_{T-1}^* that minimize the cost function for a given initial state. Consequently, these optimal actions, which can be regarded as a recipe how to operate the process such that minimal total costs incur, are encoded in the optimal value function $V_t^*: X_t \rightarrow \mathbb{R}$, which reads

$$V_t^*(x_t) = \min_{\substack{u_s \in U_s \\ s=t, \dots, T-1}} V_t(x_t, u_s, \dots, u_{T-1}). \quad (35)$$

For any given initial state, it yields the optimal remaining costs; usually, one is interested in V_0^* , i.e., the total optimal costs for the whole process. Now, it can be shown that V_t^* obeys the so-called Bellman equation [2–5], which lies at the heart of the dynamic programming paradigm and plays an important role in the field of reinforcement learning [9, 10]. It relates the optimal value function at different time steps in a recursive manner and is given by

$$V_t^*(x_t) = \min_{u_t \in U_t} \{C_t(x_t, u_t) + V_{t+1}^*(x_{t+1})\} \quad (36)$$

for $t = 0, \dots, T-1$ and all $x_t \in X_t$ with $x_{t+1} = \Gamma_t(x_t, u_t)$ and boundary condition $V_T^*(x_T) = D(x_T)$.

Solving the recursively-coupled set of equations is a non-trivial task. Fortunately, the Bellman equation suggests a practical algorithm to obtain the globally optimal solution. Typically, one is interested in the optimal control u_0^*, \dots, u_{T-1}^* of the whole process. The solution strategy consists of a backward (value) and forward (policy) iteration; see, e.g., Ref. [6]. First, one computes the function values of the optimal value function starting from the last time step and then moving sequentially backward in time, i.e., for all $t = T, \dots, 0$ and for all states $x_t \in X_t$, the values $V_t^*(x_t)$ are computed according to Eq. (36). Second, the optimal actions are obtained via

$$u_t^* = \arg \min_{u_t \in U_t} \{C_t(x_t^*, u_t) + V_{t+1}^*(\Gamma_t(x_t^*, u_t))\} \quad (37)$$

with $x_{t+1}^* = \Gamma_t(x_t^*, u_t^*)$ and initial state $x_0 = x_0^*$ for $t = 0, \dots, T-1$, i.e., forward in time.

B. Toward an optimized speed profile

In principle, the Bellman equation as given in Eq. (36) can be used right away to compute an optimized speed profile. The mapping onto that task is, for example, accomplished by the following setup:

- The trajectory of the vessel is fixed and covers a certain distance of ℓ nautical miles.

- X_t contains all feasible positions of the vessel on the trajectory (i.e., the distances traveled since departure at time $t = 0$) and environmental aspects like weather, currents, and forecasts at time t .
- U_t contains all feasible speeds (through water) of the vessel at time t .
- $C_t(x_t, u_t)$ are the fuel costs that arise if the vessel moves with speed u_t while being at position x_t at time t .
- $\Gamma_t(x_t, u_t)$ describes how a speed of u_t while being at position x_t at time t translates into a change in position to x_{t+1} .

Given that all of the above are available, particularly the cost and transition functions for arbitrary x_t and u_t , solving the Bellman equation yields optimal speeds and positions u_0^*, \dots, u_{T-1}^* and x_0^*, \dots, x_T^* , respectively, on the trajectory that globally minimize the value function, i.e., provide the optimal operating scenario for just-in-time arrival at minimal fuel consumption.

C. Proof of principle

For the purpose of a proof of principle, we choose a linear-quadratic optimal control problem. The system's dynamics are linear in both the state and action variables, while the cost functional comprises both running and terminal costs, each formulated as quadratic forms. This specific structure offers several analytical and computational advantages. First, the convexity of the cost functional and the linearity of the system's dynamics ensure that the resulting optimization problem is convex. This implies the existence of an unique global optimum. Second, the problem admits an analytical solution via the Riccati differential equation, enabling the derivation of the optimal control law in the form of a linear state feedback.

In the following, we investigate a simple implementation of what we described above in the previous subsection, namely the problem of just-in-time arrival. We set

$$X_t, U_t \subset \mathbb{R}, \quad (38)$$

$$C_t(x_t, u_t) = \left(\frac{u_t - w(x_t)}{v_{\max}} \right)^2, \quad (39)$$

$$x_{t+1} = \Gamma_t(x_t, u_t) = x_t + u_t - w(x_t), \quad (40)$$

$$D(x_T) = \alpha \left(1 - \frac{x_T}{\ell} \right)^2 + 1 \quad (41)$$

for all t .⁵ Here, $w: X_t \rightarrow \mathbb{R}$ denotes the magnitude of

the projected sea current with respect to the direction of travel at position x_t on the trajectory, v_{\max} represents the maximal possible speed through water, and $\alpha \in \mathbb{R}_{>0}$ is a numerical parameter to fine-tune the terminal costs.

Upon inserting these definitions into Eq. (34) and writing the final state as $x_T = x_s + \sum_{t=s}^{T-1} (u_t - w(x_t))$ as a sum of actions starting at time s in state x_s , which follows directly from Eq. (40), the value function for the whole process reads

$$\begin{aligned} V_s(x_s, u_s, \dots, u_{T-1}) &= \frac{1}{v_{\max}^2} \sum_{t=s}^{T-1} (u_t - w(x_t))^2 \\ &+ \alpha \left[\ell - \frac{1}{\ell} \left(x_s - \sum_{t=s}^{T-1} (u_t - w(x_t)) \right) \right]^2 \\ &+ 1. \end{aligned} \quad (42)$$

Without loss of generality (and for numerical convenience), we assume that the sets of states and actions X_t and U_t , respectively, are the same for every time step, i.e., independent of t . It is then straightforward to find the optimal actions, which are the roots of $\nabla_u V_s$ (for fixed x_s). Regarding the gradient of the value function, we find

$$\frac{\partial V_0}{\partial u_t} = \frac{2u_t}{v_{\max}^2} - \frac{2\alpha}{\ell^2} \left[\ell - x_s - \sum_{s'=s}^{T-1} (u_{s'} - w(x_{s'})) \right]. \quad (43)$$

Now, we shall solve this optimization problem by numerically solving the Bellman equation (36) and subsequently using Eq. (37) to find the optimal actions. For the sake of simplicity, we set $w(x_t) = 0$ for all $x_t \in X_t$ and all t , and consider a voyage with $\ell = 100$, $v_{\max} = 50$, and $T = 4$. Neglecting phases of (de)acceleration and without currents, the optimal solution is obviously $u_0^* = \dots = u_3^* = 25$, i.e., moving (trivially) with constant velocity. Approaching this problem in terms of the value function (41), we find from Eq. (43) the analytical solution

$$u_t^* = \frac{\alpha v_{\max}^2 (\ell - x_s)}{T - s + \ell^2} \quad (44)$$

for all $t = s, \dots, T$. As expected, this analytical solution describes a constant time-independent velocity, which consistently coincides with the optimal solution in the limit $\alpha \rightarrow \infty$, i.e., for infinite terminal costs. This analytical solution (with finite α) shall serve for comparison with results from solving the Bellman equation numerically.

In the course of that, the traditional/naive approach discretizes the state space. Hence, after the value iteration, the resulting optimal value function V_t^* is defined only on that discrete state space grid. Consequently, this poses constraints on the possible discretizations of the action space for the policy iteration (37) because for a given x_t , u_t must be chosen such that $x_{t+1} = \Gamma_t(x_t, u_t)$ lies on the state space grid, too, or the off-grid result $\Gamma_t(x_t, u_t)$ has to be “snapped” onto the nearest grid point. Both approaches induce a discretization error that manifests in the final (pseudo-)optimal policy. The in that way

⁵ From a physics point of view, u_t and w are velocities. Thus, the transition function actually reads $x_{t+1} = x_t + (u_t - w(x_t)) \Delta t$ with Δt denoting the time difference between two time steps. Since we are working solely with dimensionless quantities and integer time steps, $\Delta t = 1$ and it is omitted for the sake of brevity.

obtained optimal policy most likely differs from the true, globally-optimal solution—it is only optimal with respect to the discretization of the state space. In our case, this would result in a pseudo-optimal speed profile different from the analytical solution (44).

In principle, this issue can be mitigated by using a sufficiently dense state space grid. In our opinion, however, this is not feasible for many real-world use cases due to limitations in CPU hours and/or memory. At this point, curve fitting comes in handy. Following Ref. [10], we approximate the optimal value function in the Bellman equation for each time step separately by a linear combination of standardized functions. This is a promising approach because the optimal value function is expected to be continuous in the state variable. More precisely, for each t we write

$$\hat{V}_t^*(x_t; c) = \sum_{j=0}^{m-1} c_j^{(t)} \phi_j(x_t) \quad (45)$$

with $m \in \mathbb{N}$, and $\phi_j: X_t \rightarrow \mathbb{R}$ denote suitable standardized (basis) functions. Here, we used the circumflex notation to indicate that the optimal value function is approximated, and the superscript of the expansion coefficients emphasizes that there is a separate approximation for each time step. For the sake of brevity, we omit the dependence of \hat{V}_t^* on the coefficient vector c for the remainder of this section. The value iteration takes the same form as before (see Section IV A) but with the subtle yet important difference that the optimal value function is approximated at every time step. Starting from the end of the horizon and moving backward in time, the approximation at time step t is then used for $t-1$. We start at the finite horizon $t=T$ with the boundary condition $\hat{V}_T^*(x_T) = D(x_T)$ and then proceed backward with

$$\hat{V}_t^*(x_t) = \min_{u_t \in U_t} \{C_t(x_t, u_t) + \hat{V}_{t+1}^*(x_{t+1})\} \quad (46)$$

for $t = T-1, \dots, 0$. Here, it is worth to emphasize that at every time step, this value iteration uses only a subset of the state space due to the involved approximation, which allows for an efficient treatment of large state spaces. In the literature, this idea is also known as fitted value iteration [10]. Eventually, the resulting sequence $\hat{V}_T^*, \dots, \hat{V}_0^*$ of optimal approximated value functions is used in the usual policy iteration (37). Since these optimal value functions are now available for (in principle) arbitrary state space variables thanks to the continuous (yet fitted) nature of Eq. (45), the restrictions for the discretization of the action space are greatly relaxed.

For example, here in our specific setup, a rather fine-grained discretization of the action space could be employed in order to get close to the analytical solution. Of course, the above explained technique of a fitted value iteration applies generally to many dynamic programming problems [10] and is not restricted to our problem of an optimized speed profile.

Now, we would like to present our numerical results. We solve the Bellman equation with its ingredients given

in Eqs. ((38))–((41)). Again, we neglect currents and set $\ell = 100$, $v_{\max} = 50$, and $T = 4$. The analytical solution according to Eq. (44) is therefore given by

$$u_0^* = \dots = u_3^* = \frac{25}{1 + 1/\alpha}, \quad (47)$$

which is the optimal solution for an arbitrary $\alpha < \infty$. The Bellman equation is solved grid-based as well as with approximating the optimal value function in the sense of a fitted value iteration. For the latter, the approximation task—which is nothing but curve fitting—is accomplished classically as well as using the QUBO formulation of Section II B solved on a quantum annealer.⁶ We employ triangular functions for the expansion (45), $\phi_j = \Lambda_j$ (see Eq. (4)), with $m = 9$, $d = 9$, and $p = 8$ for the QUBO.

In the following bullet points, we summarize our solution strategies for the Bellman equation. The last three methods use a fitted value iteration as described above, where the approximation task is solved classically by matrix inversion or via a QUBO using a tabu search as well as quantum annealing. In particular, we have:

- *Analytic*: Approaching the problem in terms of the value function (41), we find from $\nabla_u V_s = 0$ (see Eq. (43)) the analytical solution.
- *Grid-based*: This baseline method avoids functional approximation entirely. Instead, the state space is discretized on a equidistant grid and estimation of the remaining costs-to-go is performed directly on grid points. It represents a brute-force approach, useful for benchmarking, but it is computationally expensive in high-dimensional state spaces.
- *Classically (matrix inversion)*: This method relies on classical linear algebra techniques. The system of equations resulting from the linear basis function ansatz is solved using Gaussian elimination. It serves as a deterministic baseline and provides exact coefficients.
- *Tabu search*: The QUBO formulation of the approximation problem is solved by a tabu search, a metaheuristic method well-suited for combinatorial landscapes. It offers a flexible alternative when exact methods are computationally unfeasible.
- *Quantum annealing*: The QUBO formulation of the approximation problem is submitted to a D-Wave quantum annealer. This explores the potential of currently available quantum annealing devices.

In Tab. V, we display our results for the optimal policies obtained by means of the different solution strategies. We have an example where the grid-based solution is indeed

⁶ Again, the *Advantage2* system but with 50 runs, 256 reads per run, and an annealing time of 1000 microseconds.

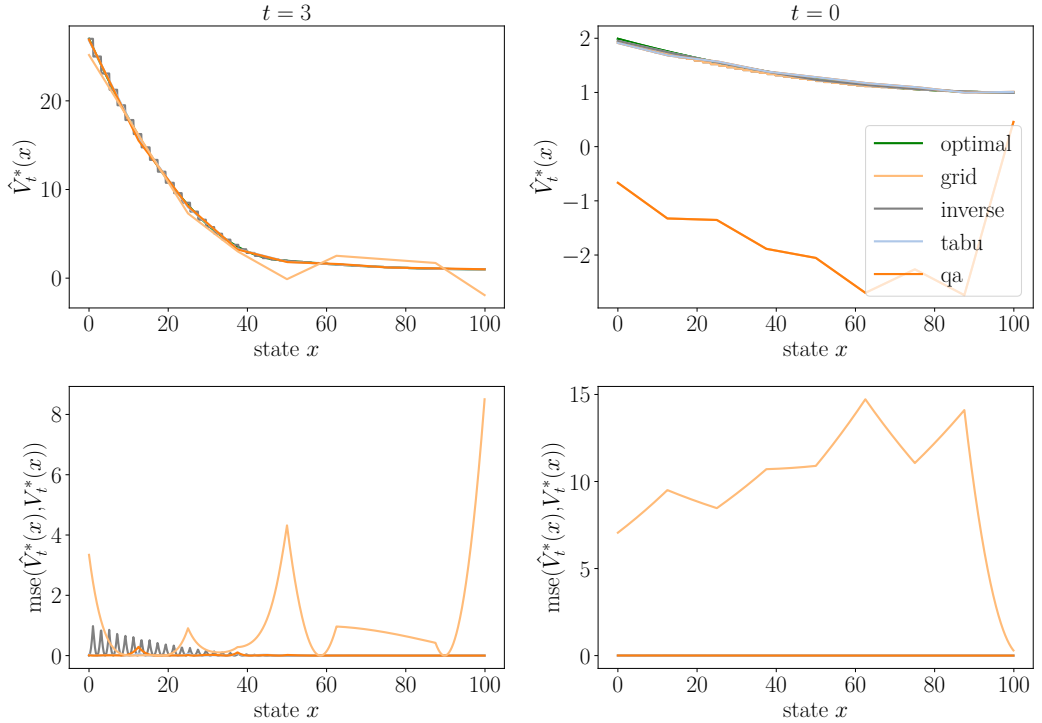


Figure 5. Visualization of the value function and approximation using different solution strategies (upper row) and their corresponding mean squared errors (MSE) (lower row). The left column shows the results for time slice $t = 3$, while the right column presents the same analysis for the first time slice $t = 0$. The upper panels depict the approximated value functions, whereas the lower panels show the associated approximation errors. Here and in the following figures, we use the MSE in contrast to the RMSE as defined in Eq. (26).

Table V. Optimal policies and their respective total costs for different solution strategies with penalty parameter $\alpha = 100$, $m = 9$, and $d = 9$.

	u_0^*	u_1^*	u_2^*	u_3^*	$V_0^*(x_0)$
analytic	24.752	2.752	24.752	24.752	1.990099
grid	23.470	24.490	24.490	26.492	1.992070
inverse	25	25	25	24.039	1.990384
tabu	25	25	25	24.039	1.990384
qa	12.5	12.5	12.5	50	2.597069

less optimal than the results that employ the fitted value iteration with the approximation solved classically by matrix inversion and QUBO-based via a tabu search. This is caused, as explained earlier, by the discretization and forcing off-grid values onto on-grid ones. Moreover, using a QUBO solved on a quantum annealer for the curve fitting in course of the fitted value iteration yields a worse optimal policy.

It should be noted that the choice of m and d results in an 81-dimensional QUBO problem. The annealer does not solve this problem size accurately enough, which is consistent with the findings in Section III. Fig. 5 shows that the solution of the quantum annealing already exhibits a significant error at the very first time slice, preventing

the method from reaching the optimal solution. Due to error propagation, this issue is further exacerbated in the subsequent time slices. The reasons lie in the size of the search space and the specific energy landscape formed by the binary representation of the coefficients.

The example calculated above does not provide a clear picture of the behavior if one varies the number of triangular functions m . Therefore, we varied the latter and analyzed the resulting errors. As shown in Fig. 6, increasing the number of basis functions leads to improved approximation results. This holds also for other values of α . At this point, all calculations shown in Fig. 6 are classical solutions of the QUBO formulation of the approximation task for \hat{V}_t^* using Gaussian elimination. Basically, this procedure corresponds to computing a matrix inverse. The resulting solution can be interpreted as the best possible outcome within the span of the chosen basis. In a following figure, we further investigate how different solvers approximate this best solution. In summary, increasing the number of basis functions effectively reduces the approximation error. The remaining challenge is to ensure that the solvers are capable of achieving this improved level of solution quality.

Our analysis shows in Fig. 7 that as the number of basis functions—and thus the problem size—increases, the solutions generally deviate further from the best possible solution, referred to as the inverse solution (indicated

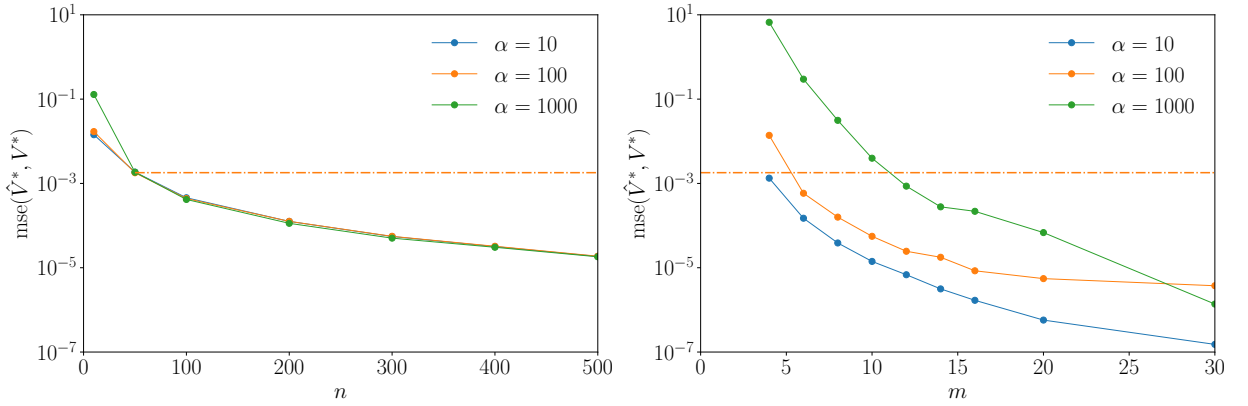


Figure 6. MSE of the reconstructed solution \hat{V}^* compared to the reference solution V^* . They carry no time index because we averaged over all time slices. Left: Convergence behavior of the MSE with respect to the number of discretization points n of the state space for different regularization parameters $\alpha \in \{10, 100, 1000\}$. Right: Error decay with respect to the number of basis functions m for fixed discretization $n = 50$ and varying α . The horizontal dashed-dotted line indicates the target error threshold, where the approximation solution with respect to the number of basis functions m starts to be more accurate than the grid solution.

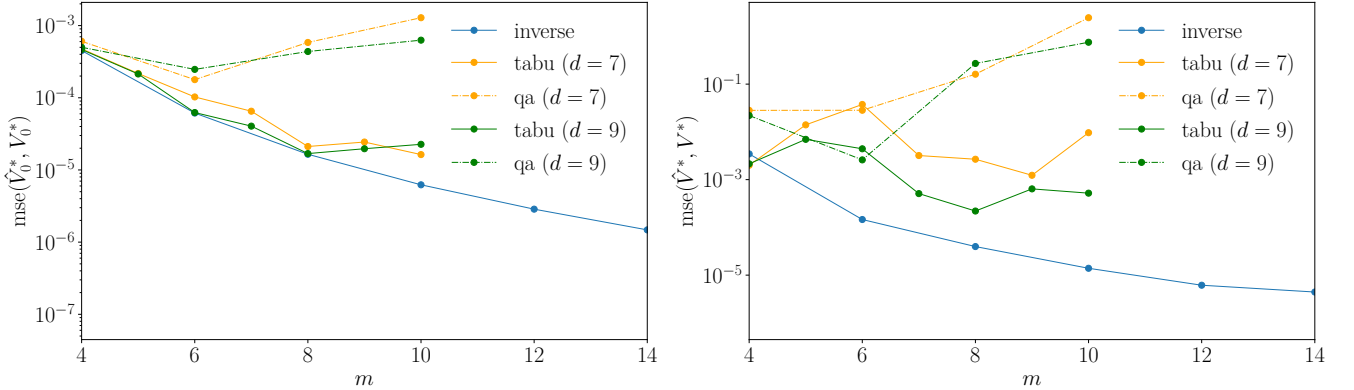


Figure 7. Error comparison of the two solution approaches, quantum annealing and tabu search, at different precision levels ($d = 7$ and $d = 9$), as a function of the number of basis functions m . The left panel shows the results for the first time slice in the fitted value iteration process, while the right panel displays the average performance over all time slices.

in blue). This trend holds for the tabu search but is especially pronounced in the case of quantum annealing. Starting from six basis functions, the problem size becomes large enough for the approximation error to increase significantly. For smaller problem sizes, the quantum annealing yields approximation results that are comparable to those obtained with the classical solution or the tabu search. However, beyond a certain problem size, this similarity breaks down as clearly illustrated in Fig. 7.

D. Further discussion

The proposed QUBO-based approach relates to a broader class of modern methods developed to approximate solutions of high-dimensional HJB equations, which typically arise in optimal control and stochastic decision problems. More specifically, we investigate a problem in the context of approximate dynamic programming

with a bounded horizon. We do not consider broader reinforcement learning techniques that incorporate policy optimization or explicit exploration-exploitation mechanisms. Furthermore, no explicit error-control strategies are employed, as our focus lies solely on the approximation quality of the value function using the QUBO approach. A central challenge in solving such equations numerically is the curse of dimensionality, i.e., the exponential growth of computational complexity with respect to the state and action space dimensions. The QUBO-based approach can be extended to multidimensional settings by employing, for example, a tensor product of basis functions.

Recent literature has addressed this challenge using learning-based strategies, most notably through the approximation of the value function or the HJB operator via deep neural networks. Notable examples include the Deep Galerkin Method [68] and physics-informed neural networks [69]. Both utilize neural networks as function approximators trained on residuals of partial differen-

tial equations. These methods are well-suited for high-dimensional spaces by leveraging the expressive capacity and scalability of deep architectures.

In contrast to these continuous, gradient-based approaches, our method introduces a discrete, combinatorial framework for function approximation based on a QUBO. This discrete optimization perspective can be interpreted as a learning approach that bypasses gradient descent and instead exploits a new perspective on value function approximation, particularly in problem settings that can be nonconvex or nondifferentiable. In such cases, the resulting value function may exhibit sharp transitions or multiple local extrema. When approximating such functions using triangular functions on a discretized grid, the associated QUBO landscape can become irregular, potentially containing many local minima. This may lead to instabilities in the QUBO optimization and reduced approximation accuracy. However, this is not an intrinsic limitation of the QUBO approach itself, but rather a structural artifact of the discretization and basis choice. In fact, quantum annealing metaheuristics, such as those employed by D-Wave, offer the potential to escape local minima via quantum tunneling, which may be advantageous in overcoming the challenges of nonconvexity.

Therefore, while nonconvexity and nondifferentiability may degrade the approximation landscape, the global nature of the QUBO formulation together with carefully chosen basis functions preserves the possibility of capturing the correct global structure of the value function.

V. SUMMARY AND CONCLUSIONS

Finding optimal speed profiles is an optimization problem that grows exponentially in time. Dynamic programming tames the combinatorial explosion of trajectories by solving the problem backward in time. The state-dependent optimal value function as a solution of the Bellman equation solves the problem linearly in the number of time steps but it requires a grid-based exploration of the entire state space. If the dimension of the latter is high, the well-known phenomena of the curse of dimensionality poses a severe obstacle, particularly for large real-world use cases. An approximation of the optimal value function and thus its continuous representation mitigates the rounding error that occurs in the discrete grid-based setup.

Such approximations can often be reduced to curve fitting in one dimension. In this work, we formulated least-squares curve fitting, where we allowed for a rather general approximator in form of a finite linear combination of standardized (basis) functions, as a QUBO that is suited to be solved with quantum annealing. For simple functions/data points, we found that quantum annealing in its current state is in principle able to deliver comparable results to a classical computer. However, curve fitting tasks that result in a QUBO size larger than roughly about 60×60 (i.e., with about 60 logical variables or

more) cannot be solved accurate enough on a D-Wave annealer yet. The reason for that is the difficult low-energy landscape of the resulting Ising Hamiltonian. Moreover, QUBO problems described by global basis functions (e.g., Chebyshev polynomials) are even more difficult to solve, hence even smaller problems can have a poor solution quality.

In general, optimization problems formulated in terms of a QUBO can be modified by fine-tuning the penalty coefficients of the constraints in order to manipulate these landscapes in a proper way [70]. In our case, however, such an approach is not possible because the values of the QUBO matrix entries are solely fixed by the to-be-approximated data and the basis functions used for the approximator. Furthermore, the embedding of a floating point number on a quantum annealer might also contribute to an already complicated low-energy landscape.

Though quantum annealing devices promise a large number of qubits, attention should be paid to how many direct connections exist between the physical qubits. If one needs many interconnected variables, logical qubits must be created from several physical ones. We found that basis functions with support on the whole real line, e.g., all polynomials, result in a highly-connected QUBO matrix that is difficult to embed into the working graph of the annealer. However, we are confident that this issue will vanish eventually in the near future because of the advances in the ongoing development of quantum annealing hardware.

Nevertheless, the quantum annealing-oriented curve fitting principally works. Regarding a real-world use case—albeit still in an exploratory fashion—we investigated the linear-quadratic optimal control problem of just-in-time arrival of a vessel, where we approximated the value function in the Bellman equation. With an increasing number of basis functions, the solution space can be better represented, leading to more accurate value estimates compared to the grid-based method. Nevertheless, there was hope that the quantum annealing process would yield lower errors in larger search spaces. Unfortunately, we find that D-Wave’s current quantum annealing hardware does not yet appear to be capable of meeting this expectation.

ACKNOWLEDGMENTS

We acknowledge funding and support from the German Federal Ministry for Economic Affairs and Climate Action (Bundesministerium für Wirtschaft und Klimaschutz) through the PlanQK initiative (01MK20005).

This project (HA project no. 1362/22-67) is financed with funds of LOEWE—Landes-Offensive zur Entwicklung Wissenschaftlich-ökonomischer Exzellenz, Förderlinie 3: KMU-Verbundvorhaben (State Offensive for the Development of Scientific and Economic Excellence).

DECLARATIONS

Author contributions

Conceptualization, funding acquisition, and supervision: B. Harrach and W. Mergenthaler. Formal analysis, investigation, and software: P. Isserstedt and D. Jaroszewski. Validation: P. Isserstedt, D. Jaroszewski, and F. Paul. Writing (original draft): P. Isserstedt and

D. Jaroszewski. Writing (review and editing): P. Isserstedt, D. Jaroszewski, and F. Paul. This list uses the Contributor Role Taxonomy (CRediT) [71].

Competing interests

The authors have no competing interests to declare that are relevant to the content of this article.

[1] GEF-UNDP-IMO GloMEEP Project and members of the GIA, *Just In Time Arrival Guide—Barriers and Potential Solutions* (GloMEEP Project Coordination Unit, International Maritime Organization, 2020).

[2] R. Bellman, On the Theory of Dynamic Programming, *Proc. Natl. Acad. Sci. USA* **38**, 716 (1952).

[3] R. Bellman, Some Functional Equations in the Theory of Dynamic Programming, *Proc. Natl. Acad. Sci. USA* **39**, 1077 (1953).

[4] R. Bellman, Dynamic Programming and a New Formalism in the Calculus of Variations, *Proc. Natl. Acad. Sci. USA* **40**, 231 (1954).

[5] R. Bellman, *Dynamic Programming* (Princeton University Press, 1957).

[6] K. Neumann and M. Morlock, *Operations Research*, 2nd ed. (Hanser, 2002).

[7] D. P. Bertsekas, *Dynamic Programming and Optimal Control—Volume I*, 4th ed. (Athena Scientific, 2017).

[8] D. P. Bertsekas, *Dynamic Programming and Optimal Control—Volume II*, 4th ed. (Athena Scientific, 2012).

[9] R. S. Sutton and A. G. Barto, *Reinforcement Learning: An Introduction*, 2nd ed. (MIT Press, 2018).

[10] D. P. Bertsekas, *Reinforcement Learning and Optimal Control* (Athena Scientific, 2019).

[11] M. G. Lagoudakis, Value Function Approximation, in *Encyclopedia of Machine Learning*, edited by C. Sammut and G. I. Webb (Springer, 2010).

[12] G. Kochenberger *et al.*, The unconstrained binary quadratic programming problem: a survey, *J. Comb. Optim.* **28**, 58 (2014).

[13] F. Glover, G. Kochenberger, and Y. Du, A Tutorial on Formulating and Using QUBO Models, [arXiv:1811.11538 \[cs.DS\]](https://arxiv.org/abs/1811.11538) (2014).

[14] B. Apolloni, C. Carvalho, and D. de Falco, Quantum stochastic optimization, *Stoch. Process. Appl.* **33**, 233 (1989).

[15] T. Kadowaki and H. Nishimori, Quantum annealing in the transverse Ising model, *Phys. Rev. E* **58**, 5355 (1998), [arXiv:cond-mat/9804280](https://arxiv.org/abs/cond-mat/9804280).

[16] J. Brooke, D. Bitko, T. F. Rosenbaum, and G. Aeppli, Quantum Annealing of a Disordered Magnet, *Science* **284**, 779 (1999), [arXiv:cond-mat/0105238](https://arxiv.org/abs/cond-mat/0105238).

[17] E. Farhi, J. Goldstone, S. Gutmann, and M. Sipser, Quantum Computation by Adiabatic Evolution, [arXiv:quant-ph/0001106](https://arxiv.org/abs/quant-ph/0001106) (2000).

[18] E. Farhi *et al.*, A Quantum Adiabatic Evolution Algorithm Applied to Random Instances of an NP-Complete Problem, *Science* **292**, 472 (2001), [arXiv:quant-ph/0104129](https://arxiv.org/abs/quant-ph/0104129).

[19] E. Farhi, J. Goldstone, and S. Gutmann, Quantum Adiabatic Evolution Algorithms versus Simulated Annealing, [arXiv:quant-ph/0201031](https://arxiv.org/abs/quant-ph/0201031) (2002).

[20] D. Aharonov *et al.*, Adiabatic Quantum Computation is Equivalent to Standard Quantum Computation, *SIAM J. Comput.* **37**, 166 (2007), [arXiv:quant-ph/0405098](https://arxiv.org/abs/quant-ph/0405098).

[21] R. D. Somma, D. Nagaj, and M. Kieferová, Quantum Speedup by Quantum Annealing, *Phys. Rev. Lett.* **109**, 050501 (2012), [arXiv:1202.6257 \[quant-ph\]](https://arxiv.org/abs/1202.6257).

[22] A. Lucas, Ising formulation of many NP problems, *Front. Phys.* **2**, 5 (2014), [arXiv:1302.5843 \[cond-mat.stat-mech\]](https://arxiv.org/abs/1302.5843).

[23] Z. Bain *et al.*, Discrete optimization using quantum annealing on sparse Ising models, *Front. Phys.* **2**, 56 (2014).

[24] C. C. McGeoch, *Adiabatic Quantum Computation and Quantum Annealing: Theory and Practice* (Morgan & Claypool, 2014).

[25] T. Albash and D. A. Lidar, Adiabatic quantum computation, *Rev. Mod. Phys.* **90**, 015002 (2018), [arXiv:1611.04471 \[quant-ph\]](https://arxiv.org/abs/1611.04471).

[26] S. E. Venegas-Andraca, W. Cruz-Santos, C. C. McGeoch, and M. Lanzagorta, A cross-disciplinary introduction to quantum annealing-based algorithms, *Contemp. Phys.* **59**, 174 (2018), [arXiv:1803.03372 \[quant-ph\]](https://arxiv.org/abs/1803.03372).

[27] S. Yarkoni, E. Raponi, T. Bäck, and S. Schmitt, Quantum annealing for industry applications: introduction and review, *Rep. Prog. Phys.* **85**, 104001 (2022), [arXiv:2112.07491 \[quant-ph\]](https://arxiv.org/abs/2112.07491).

[28] A. J. Berkeley *et al.*, A scalable readout system for a superconducting adiabatic quantum optimization system, *Supercond. Sci. Technol.* **23**, 105014 (2010), [arXiv:0905.0891 \[cond-mat.supr-con\]](https://arxiv.org/abs/0905.0891).

[29] M. W. Johnson *et al.*, A scalable control system for a superconducting adiabatic quantum optimization processor, *Supercond. Sci. Technol.* **23**, 065004 (2010), [arXiv:0907.3757 \[quant-ph\]](https://arxiv.org/abs/0907.3757).

[30] R. Harris *et al.*, Experimental demonstration of a robust and scalable flux qubit, *Phys. Rev. B* **81**, 134510 (2010), [arXiv:0909.4321 \[cond-mat.supr-con\]](https://arxiv.org/abs/0909.4321).

[31] R. Harris *et al.*, Experimental investigation of an eight-qubit unit cell in a superconducting optimization processor, *Phys. Rev. B* **82**, 024511 (2010), [arXiv:1004.1628 \[cond-mat.supr-con\]](https://arxiv.org/abs/1004.1628).

[32] M. W. Johnson *et al.*, Quantum annealing with manufactured spins, *Nature* **473**, 194 (2011).

[33] N. Dickson *et al.*, Thermally assisted quantum annealing of a 16-qubit problem, *Nature Commun.* **4**, 1903 (2013).

[34] S. Boixo *et al.*, Evidence for quantum annealing with more than one hundred qubits, *Nature Phys.* **10**, 218 (2014), [arXiv:1304.4595 \[quant-ph\]](https://arxiv.org/abs/1304.4595).

[35] T. Lanting *et al.*, Entanglement in a Quantum Annealing Processor, *Phys. Rev. X* **4**, 021041 (2014), arXiv:1401.3500 [quant-ph].

[36] P. I. Bunyk *et al.*, Architectural Considerations in the Design of a Superconducting Quantum Annealing Processor, *IEEE Trans. Appl. Supercond.* **24**, 1700110 (2014), arXiv:1401.5504 [quant-ph].

[37] C. C. McGeoch, R. Harris, S. P. Reinhardt, and P. I. Bunyk, Practical Annealing-Based Quantum Computing, *Computer* **52**, 38 (2019).

[38] O. Parekh *et al.*, Benchmarking Adiabatic Quantum Optimization for Complex Network Analysis, arXiv:1604.00319 [quant-ph] (2016).

[39] M. Jünger *et al.*, Quantum Annealing versus Digital Computing: An Experimental Comparison, *ACM J. Exp. Algorithms* **26**, 1.9:1 (2021).

[40] Z. R. Lin *et al.*, Josephson parametric phase-locked oscillator and its application to dispersive readout of superconducting qubits, *Nature Commun.* **5**, 4480 (2014).

[41] NEC develops the world's first unit cell facilitating scaling up to a fully-connected quantum annealing architecture, https://www.nec.com/en/press/202203/global_20220317_01.html (2022), accessed on 2025-03-17.

[42] Tohoku University and NEC start joint research on computer systems using a newly developed 8-qubit quantum annealing machine, https://www.nec.com/en/press/202306/global_20230628_01.html (2023), accessed on 2025-03-17.

[43] V. Canivell, P. Forn-Díaz, A. García-Saez, and R. Sagastizabal, Startup Qilimanjaro—towards a European full-stack coherent quantum annealer platform, *EPJ Quantum Technol.* **8**, 6 (2021).

[44] A. Palacios, A. García-Saez, and M. P. Estarellas, A scalable 2-local architecture for quantum annealing of Ising models with arbitrary dimensions, arXiv:2404.06861 [quant-ph] (2024).

[45] T. Inagaki *et al.*, A coherent Ising machine for 2000-node optimization problems, *Science* **354**, 603 (2016).

[46] P. L. McMahon *et al.*, A fully programmable 100-spin coherent Ising machine with all-to-all connections, *Science* **354**, 614 (2016).

[47] A. Quarteroni, R. Sacco, and F. Saleri, *Numerical Mathematics*, 2nd ed. (Springer, 2007).

[48] G. Eichmann, H. Sanchis-Alepuz, R. Williams, R. Alkofer, and C. S. Fischer, Baryons as relativistic three-quark bound states, *Prog. Part. Nucl. Phys.* **91**, 1 (2016), arXiv:1606.09602 [hep-ph].

[49] H. Sanchis-Alepuz and R. Williams, Recent developments in bound-state calculations using the Dyson–Schwinger and Bethe–Salpeter equations, *Comput. Phys. Commun.* **232**, 1 (2018), arXiv:1710.04903 [hep-ph].

[50] F. Olver, D. Lozier, R. Boisvert, and C. Clark, *The NIST Handbook of Mathematical Functions* (Cambridge University Press, 2010).

[51] A. Ben-Israel and T. N. E. Greville, *Generalized Inverses: Theory and Applications*, 2nd ed. (Springer, 2003).

[52] F. Glover, Tabu Search—Part I, *ORSA J. Comput.* **1**, 190 (1989).

[53] F. Glover, Tabu Search—Part II, *ORSA J. Comput.* **2**, 4 (1990).

[54] D-Wave Documentation, <https://docs.dwavesys.com/docs/latest/index.html> (2025), accessed on 2025-02-04.

[55] E. Ising, Beitrag zur Theorie des Ferromagnetismus, *Z. Phys.* **31**, 253 (1925).

[56] C. Itzykson and J.-M. Drouffe, *Statistical Field Theory—Volume 1: From Brownian Motion to Renormalization and Lattice Gauge Theory* (Cambridge University Press, 1989).

[57] G. Palubeckis, Multistart Tabu Search Strategies for the Unconstrained Binary Quadratic Optimization Problem, *Ann. Oper. Res.* **131**, 259 (2004).

[58] M. Lewis and F. Glover, Quadratic unconstrained binary optimization problem preprocessing: Theory and empirical analysis, *Networks* **70**, 79 (2017).

[59] F. Glover, M. Lewis, and G. Kochenberger, Logical and inequality implications for reducing the size and difficulty of quadratic unconstrained binary optimization problems, *Eur. J. Op. Res.* **265**, 829 (2018), arXiv:1705.09545 [cs.AI].

[60] V. Suppakitpaisarn and J.-K. Hao, Utilizing Graph Sparification for Pre-processing in Maxcut QUBO Solver, arXiv:2401.13004 [math.OC] (2024).

[61] E. S. Tiunov, A. E. Ulanov, and A. I. Lvovsky, Annealing by simulating the coherent Ising machine, *Optics Express* **27**, 8505 (2019), arXiv:1901.08927 [quant-ph].

[62] Y. Du *et al.*, New advances for quantum-inspired optimization, *Intl. Trans. Op. Res.* **32**, 6 (2025).

[63] R. Hamerly *et al.*, Experimental investigation of performance differences between Coherent Ising Machines and a quantum annealer, *Sci. Adv.* **5**, 1 (2019), arXiv:1805.05217 [quant-ph].

[64] H. Takesue *et al.*, Finding independent sets in large-scale graphs with a coherent Ising machine, *Sci. Adv.* **11**, 1 (2025).

[65] R. Ferretti and A. Festa, A hybrid control approach to the route planning problem for sailing boats, arXiv:1707.08103 [math.NA] (2017).

[66] C. Miles and A. Vladimirs, Stochastic Optimal Control of a Sailboat, arXiv:2109.08260 [math.OC] (2021).

[67] M. Wang, N. Patnaik, A. Somalwar, J. Wu, and A. Vladimirs, Risk-aware stochastic control of a sailboat, arXiv:2309.13436 [math.OC] (2023).

[68] J. Sirignano and K. Spiliopoulos, DGM: A deep learning algorithm for solving partial differential equations, *J. Comput. Phys.* **375**, 1339 (2018), arXiv:1708.07469 [q-fin.MF].

[69] M. Raissi, P. Perdikaris, and G. E. Karniadakis, Physics-informed neural networks: A deep learning framework for solving forward and inverse problems involving nonlinear partial differential equations, *J. Comput. Phys.* **378**, 686 (2019).

[70] C. Roch, D. Ratke, J. Nüßlein, T. Gabor, and S. Feld, The Effect of Penalty Factors of Constrained Hamiltonians on the Eigenspectrum in Quantum Annealing, *ACM Trans. Quant. Comput.* **4**, 1 (2023).

[71] Contributor Role Taxonomy, <https://credit.niso.org/> (2025), accessed on 2025-06-27.